Steady late quaternary slip rate on the Cinarcik section of the North Anatolian fault near Istanbul, Turkey

Hulya Kurt,[1] C. C. Sorlien,[2] L. Seeber,[3] M. S. Steckler,[3] D. J. Shillington,[3] G. Cifci,[4] M.-H. Cormier,[5,6] J.-X. Dessa,[7] O. Atgin,[4] D. Dondurur,[4] E. Demirbag,[1] S. Okay,[4] C. Imren,[1] S. Gurcay,[4] and H. Carton[3]

Received 15 June 2013; revised 13 August 2013; accepted 15 August 2013; published 3 September 2013.

[1] The distribution of plate motion between multiple fault strands and how this distribution may evolve remain poorly understood, despite the key implications for seismic hazards. The North Anatolian Fault in northwest Turkey is a prime example of a multistranded continental transform. Here we present the first constraints on late Quaternary slip rates on its northern branch across the Cinarcik Basin in the eastern Marmara Sea. We use both deep penetration and high-resolution multichannel seismic reflection data with a stratigraphic age model to show that a depocenter has persisted near the fault bend responsible for that transform basin. Successively older depocenters have been transported westward by fault motion relative to Eurasia, indicating a uniform right-lateral slip rate of 18.5 mm/yr over the last 500,000 years, compared to overall GPS rates (23–24 mm/yr). Thus, the northern branch has slipped at a nearly constant rate and has accounted for most of the relative plate motion between Eurasia and Anatolia since ~0.5 Ma.
Citation: Kurt, H., et al. (2013), Steady late quaternary slip rate on the Cinarcik section of the North Anatolian fault near Istanbul, Turkey, *Geophys. Res. Lett.*, *40*, 4555–4559, doi:10.1002/grl.50882.

1. Introduction

[2] Plate motion at continental transforms, such as the San Andreas Fault in southern California and the North Anatolian Fault (NAF) in western Turkey, can be distributed across several fault strands spanning hundreds of kilometers. While overall plate motion is commonly steady over millions of years, the partitioning of that motion among multiple fault strands may change with time, as documented by the comparison of modern geodetic rates versus Holocene slip rates along certain faults. Current evidence comes from differences in modern versus Holocene slip rates along specific faults [*Polonia et al.*, 2004; *Dolan et al.*, 2007; *Frankel et al.*, 2011]. However, little is known about how slip-rate changes along and between strands on timescales of a few hundred thousand years, in part because precise stratigraphic age models have been lacking beyond the ~40 ka age range of radiocarbon dating.

[3] The NAF between the Anatolian and Eurasian plates accommodates 23–24 mm/yr of dextral motion [*Reilinger and McClusky*, 2011], primarily by recurrent large earthquakes [*Barka and Kadinsky-Cade*, 1988; *Ambraseys and Jackson*, 2000]. These earthquakes, such as the M7.4 near Izmit in 1999, are often disastrous to population centers in northern Turkey. The 1500 km long NAF splits into three major branches in northwest Turkey (Figure 1), and most of the strain accumulation is thought to occur on the northern branch (NAF-N) that bisects the Marmara Sea. The Marmara Sea comprises a series of actively subsiding basins forming along the NAF-N. Numerous competing models for fault configuration and temporal evolution have been proposed to account for its formation, evolution, and historic seismicity [*Barka and Kadinsky-Cade*, 1988; *Ambraseys and Finkel*, 1995; *Okay et al.*, 2000; *Le Pichon et al.*, 2001; *Armijo et al.*, 2002; *Seeber et al.*, 2004; *Seeber et al.*, 2006].

[4] Here we address two long-standing questions regarding the Marmara Sea that have broad implications for continental transform fault systems worldwide. (1) How is deformation distributed between the faults branches beneath Marmara Sea? Most studies agree that the NAF-N accommodates a large portion of the motion, but it is unclear to what extent the two other branches of the NAF might participate in accommodating some of this strike-slip motion or in forming the basins of the Marmara Sea. Some authors propose partitioning of motion between strike-slip and normal faults, and that the latter creates the basins [*Armijo et al.*, 2002; *Le Pichon et al.*, 2003; *Carton et al.*, 2007]. (2) Also, has fault configuration and kinematics changed through time or has deformation occurred in a steady state mode on the same structures that are active today? Existing models propose steady state slip on a nonvertical transform [*Seeber et al.*, 2004, 2006] or a pull-apart configuration [*Armijo et al.*, 2002]. Another model calls for the formation of a pure strike-slip fault in the last ~200 ka, cutting through and deactivating the pull-apart basins [*Le Pichon et al.*, 2001, 2003; *Rangin et al.*, 2004].

[5] Addressing the questions above requires temporal constraints on slip rates for NAF-N and other faults. Currently, constraints are limited to modern rates across the entire Marmara Basin from geodetic data and rates estimated for the Holocene from paleoseismology [*Meghraoui et al.*, 2012]. Holocene rates of right-lateral slip across the NAF-N to the east of the Marmara Sea in Izmit Gulf and its eastern part onshore are smaller than the modern rates inferred from GPS

Additional supporting information may be found in the online version of this article.

[1]Department of Geophysical Engineering, Istanbul Technical University, Istanbul, Turkey.
[2]University of California, Santa Barbara, California, USA.
[3]Lamont-Doherty Earth Observatory of Columbia University, Palisades, New York, USA.
[4]Dokuz Eylul University, Izmir, Turkey.
[5]University of Missouri, Columbia, Missouri, USA.
[6]Now at University of Rhode Island, Graduate School of Oceanography, Kingston, Rhode Island, USA.
[7]Geoazur, Observatoire de la Cote d'Azur, University Pierre et Marie Curie, Valbonne, France.

Corresponding author: H. Kurt, Department of Geophysical Engineering, Istanbul Technical University, Maslak, Istanbul 34469, Turkey. (kurt@itu.edu.tr)

0094-8276/13/10.1002/grl.50882

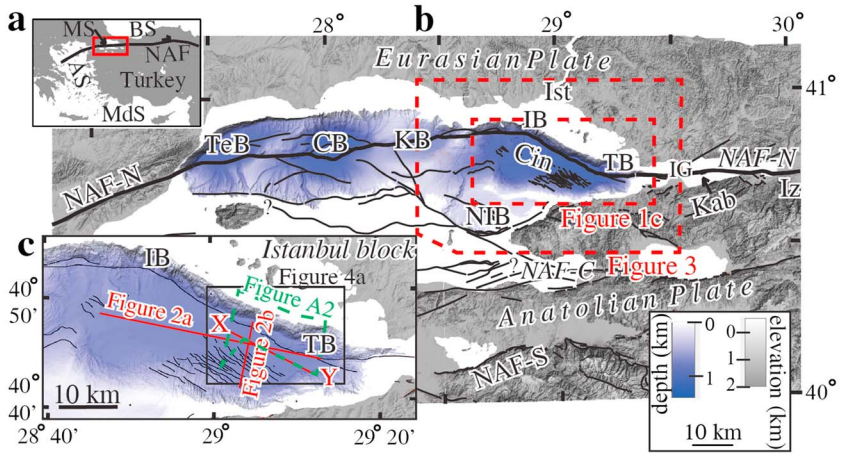

Figure 1. Bathymetry [*Rangin et al*., 2001], Shuttle Radar Topography Mission topography, and tectonic setting of the Marmara Sea region including Cinarcik Basin ("Cin"). (a) Location of Figure 1b in northwest Turkey given by the rectangle. MS, BS, AS, and MdS are Marmara Sea, Black Sea, Aegean Sea, and Mediterranean Sea, respectively. NAF is North Anatolian Fault. (b) Onshore and SE Marmara Sea faults from *Gasperini et al*. [2011] and *Emre et al*. [2012]. Offshore faults are modified from *Sorlien et al*. [2012]. NAF-N, NAF-C, and NAF-S are Northern, Central, and Southern branches of the North Anatolian Fault, respectively. TeB, CB, KB, NIB, KB, Cin, and Kab are Tekirdag, Central, Kumburgaz, North Imrali, Karamursel, Cinarcik, and Karamursel basins. TB and IB are Tuzla and Istanbul bends. IG, Iz, and Ist are Izmit Gulf and cities of Izmit and Istanbul, respectively. Dashed polygons indicate locations of other figures. (c) Detailed view of Cinarcik Basin with faults and bathymetry. Locations of seismic profiles and figures are indicated.

strain accumulation [*Polonia et al*., 2004; *Kozaci et al*., 2009]. Here we apply a stratigraphic age model to a dense grid of offshore seismic reflection profiles to unravel the evolution of one of the Marmara basins over the past 540 ka. Cinarcik Basin, the easternmost basin in the Marmara Sea, is associated with a major bend of the fault (Figure 1). We show that its growth results from oblique right-normal displacement on the NAF-N and that the slip rate has been overall steady for the past 540 ka, at circa 100 ka resolution.

2. Material and Methods

[6] A dense grid of multichannel seismic (MCS) profiles with a wide range of resolution and penetration were used for this study. This multiresolution data set has allowed us

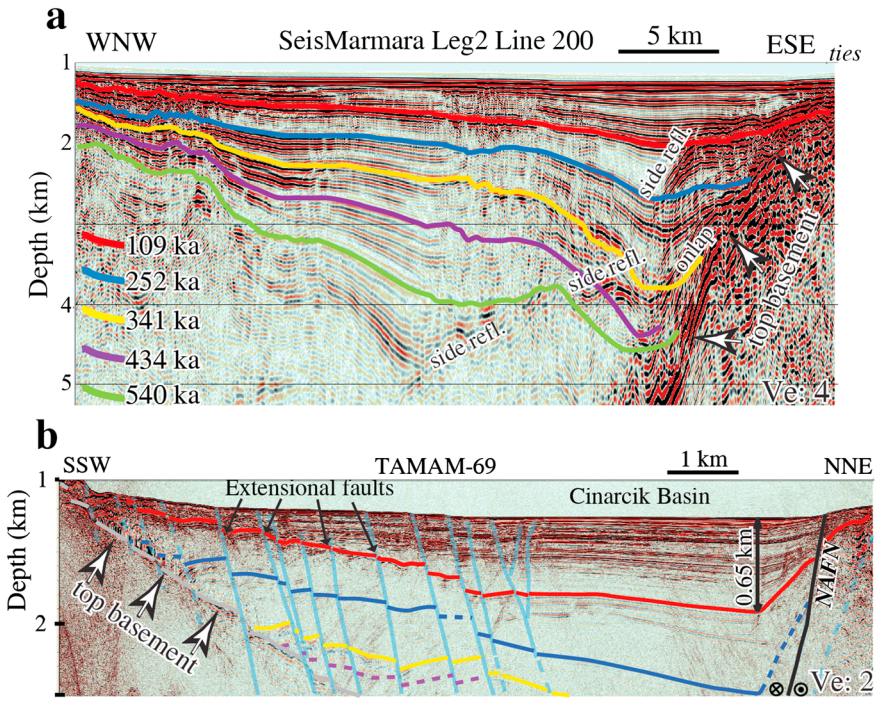

Figure 2. Migrated depth sections of Cinarcik Basin, located on Figure 1. (a) Oblique strike section SM-200 with five horizons. The ages of the horizons are given on the left below [*Sorlien et al*., 2012]. Tick marks along the top represent intersections of other profiles used in interpretation. The onlap in the east is successively farther west for older horizons. (b) TAMAM-69. Extension across the Red-1 horizon was measured from the normal-separation faults.

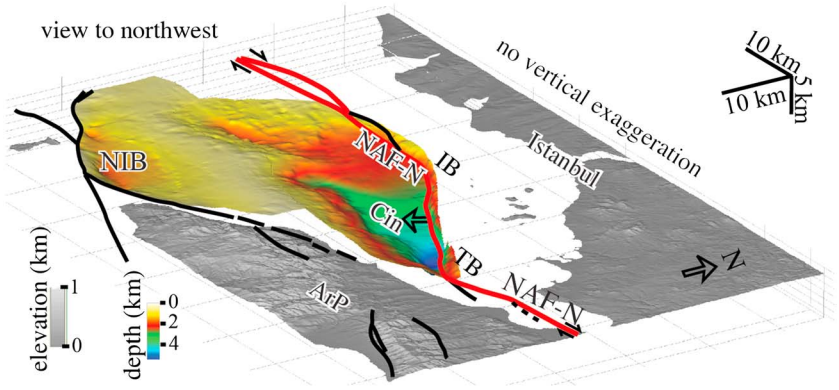

Figure 3. Oblique view to NW of the Green-6 horizon. Note how the deepest part of the 540 ka Green-6 sedimentary basin occurs near Tuzla bend (TB). The thick arrow gives NAF-N SSW dip direction. NIB and Cin are North Imrali and Cinarcik basins. NAF-N, IB, and ArP are northern branch of the North Anatolian Fault, Istanbul bend, and Armutlu Peninsula, respectively.

to resolve critical details at shallow depth and then continue our interpretation to older and deeper strata. Detailed processing information and examples for this diverse data set can be found in *Okay et al*. [2000], *Carton et al*. [2007], *Sorlien et al*. [2012], and *Shillington et al*. [2012]. Seafloor morphology is derived from a 20 m grid of multibeam bathymetry [*Le Pichon et al*., 2001; *Rangin et al*., 2001].

[7] Seismic horizons were mapped using standard loop-tying techniques for all the 2-D data shown in the track maps and in the preceding references with the interpretation software *Kingdom Suite of Information Handling Services (IHS)*. The abundance of both strike and dip profiles allowed for loop ties at many intersections and thus multiple opportunities to test interpretations and highlight possible errors. The traced horizons, from younger to older, include Red-1, Blue-2, Yellow-4, Violet-5, and Green-6 (Figure 2), following the same color convention as *Sorlien et al*. [2012]. Smooth horizon surfaces in two-way traveltime were gridded at 100 m spacing.

[8] To convert the seismic horizons to depth, we constructed a 3-D velocity model for Cinarcik Basin. MCS stacking velocities of the Turkish-American MArmara Multichannel (TAMAM) project were used to derive interval velocities for the shallow sediments. At depth, refraction velocities [*Dessa et al*., 2007] determined along the SeisMarmara Leg 2 profiles constrained interval velocities of 2.5 km/s and higher. Velocities between the shallow sediments and the 2.5 km/s refraction velocities were linearly interpolated. Differential depths between successive horizons, including the seafloor, yielded isochores (vertical thickness) and the total sediment volumes between them (Figure S1). In order to compare sediment accumulation at different stages of basin development, we corrected thicknesses for sediment compaction. To that end, we used the velocity model to estimate density [*Brocher*, 2005] and then inferred porosity based on an assumed grain density of 2.68 g/cm^2. Lastly, we integrated to estimated sediment mass and the decompacted volume of sediments, i.e., the thickness of sediments in each horizon, as if they had maintained constant porosities.

[9] Dense refraction data do not exist from North Imrali Basin and a 1-D velocity function was used for depth conversions there [*Sorlien et al*., 2012]. If the sediment flux into the combined North Imrali-Cinarcik basins had been constant through time on a 100 ka timescale, and the published age model is correct, we would expect to see a linear cumulative volume curve. Instead, Figure S1 suggests a marked decrease in sediment flux at, or soon after, deposition of Blue-2, at around ~250 ka.

3. Steady Westward Migration of Cinarcik Basin

[10] The Cinarcik Basin is adjacent to the ~30 km long releasing segment of the NAF-N between the Tuzla and the Istanbul bends (Figure 1). Precise mapping of five seismic horizons (Figure 2) shows that the basin is strongly asymmetric in shape and growth patterns. It narrows toward the east near the Tuzla bend (Figures 1, 2, and 3). This narrow end is the deepest part of the bathymetric basin, but also the youngest, and most rapidly subsiding part of the sedimentary basin. In addition, the turbiditic sediments on the basin floor have been steadily onlapping the eastern flank of the basin (Figure 2a). This asymmetry and time-transgressive behavior have been recognized as characteristic of basins that form on the releasing sides of bends on strike-slip faults [*Seeber et al*., 2010]. Examples include the classic Ridge Basin in California [*Crowell*, 2003], basins along the NAF-N (e.g., Tekirdag Basin in western Marmara Sea) [*Seeber et al*., 2004], and the Karamursel Basin in Izmit Gulf [*Cormier et al*., 2006; *Kurt and Yucesoy*, 2009] (Figure 1).

[11] An evolutionary model for transform basins that can account for the above features of Cinarcik Basin [*Seeber et al*., 2010] assumes two controlling elements. First, the geometry of the nonvertical fault through the releasing bend is stable and stationary relative to one side of the fault, which is thus not required to deform internally. The other side moves at transform speed relative to the bend and deforms internally to accommodate the bend and the releasing component of motion. In our case, the Tuzla bend on the NAF-N at the eastern end of the Cinarcik Basin (Figures 1 and 3) is fixed to the relatively stable Istanbul block (Eurasian plate) north of the NAF-N, while the deformation to accommodate the bend, including basin growth, is relegated to the south side of the NAF-N. In this and other examples, the fault dips toward the basin (Figure 2b), and the footwall is the stable side of the fault. In this time-transgressive system, the active Cinarcik depocenter, located on the south side of the fault maintains a fixed position relative to the north side of the NAF-N, while sediments deposited at that position migrate westward at the transform speed relative to the bend and the footwall. Our stratigraphic analysis constrains the growth of the Cinarcik Basin both spatially and temporally (Figure 4), (Figure S2), revealing a pattern that is indeed compatible with the above model. The westward migration of progressively older depocenters relative to the northern Istanbul footwall block is

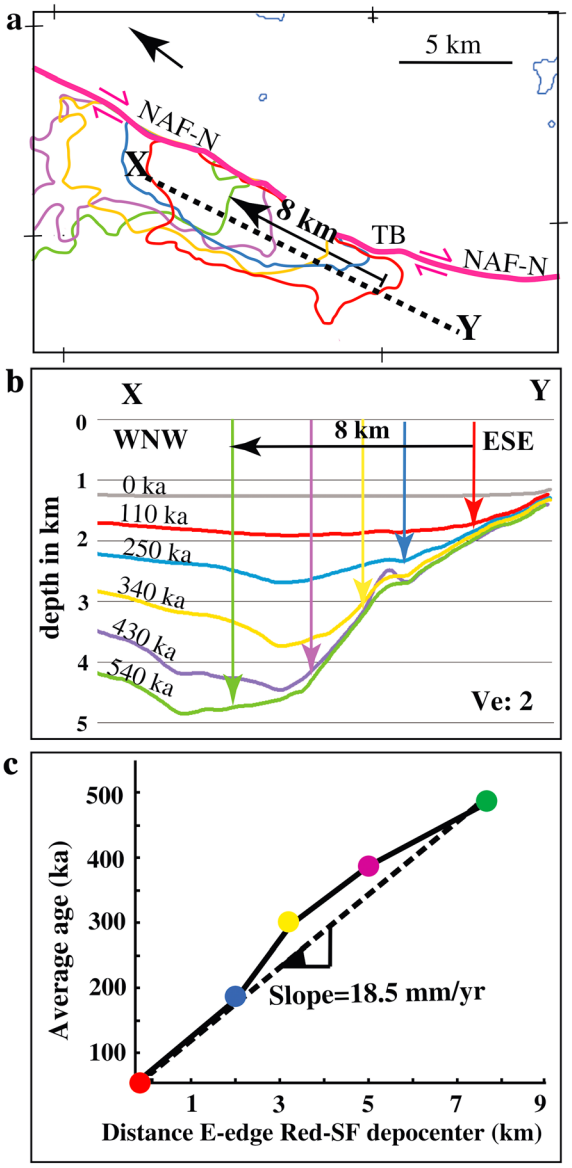

Figure 4. Moving depocenter. (a) The 500 m thickness contours of each isochore (vertical thickness). Color corresponds to the age at the base of each interval, as labeled in Figure 4b. *X-Y* locates the cross section displayed on Figure 4b. TB is Tuzla bend. (b) Cross-section *X-Y* through the depth model, displayed with 2× vertical exaggeration (Ve) and located on Figure 1c. Arrows indicate the eastside of the 500 m isochore contour. The distance between the Red-1 to seafloor arrow and Green-6 to Violet-5 arrow is about 8 km. (c) Average age of each interval versus distance from the east edge of the youngest (red) isochore 500 m contour. The color of each dot corresponds to the horizon at the base of each interval. The relation between average age and distance is nearly linear, indicating steady state deformation.

approximately proportional to their age and is interpreted to represent the dextral motion on the NAF-N in eastern Cinarcik (Figure S3 and Text S1). Our preferred slip rate over the last 0.49 Ma is 18.5 + 10.9/− 5.9 mm/yr (Figure 4). Uncertainties include 100 ka in the age of the Blue-2 and older horizons (due to assignment of the glacial cycles), and 1 km in the position of the measured eastern edge of each depocenter. This compares to a right-lateral rate of 17 ± 5 mm/yr for the last 1000 years across the Ganos fault just west of Marmara Sea, from paleoseismology [*Meghraoui et al.*, 2012].

[12] The second element of this transform-bend basin hypothesis is that the extension is accommodated mostly by the transform fault itself and is not substantially partitioned, at least near the Tuzla bend. The main agent of eastern Cinarcik Basin growth is oblique normal slip on the south-dipping NAF-N, which essentially serves as both the transform boundary and the border fault of the basin. Thus, the rate of oblique true slip is higher than the rate of right-lateral motion reported above. The observed pattern of subsidence accounts for the asymmetric growth of the Cinarcik Basin. Indeed, in the eastern half of the basin, the turbiditic beds are progressively obliquely tilted down to the northeast, toward the NAF-N. Figure 2 shows the two components of this tilt, one to the NNE and the other to the ESE, approximately perpendicular and parallel to the NAF-N, respectively. This tilt requires a normal component on the dextral south-dipping NAF-N that is responsible for subsidence at the eastern end of the basin. The obliquity of the tilt shows that the rate of subsidence decreases westward from the bend. Relative to the current seafloor morphology and to the southern onlap, the 109 ka old Red-1 horizon in Figure 2b is tilted about 4° and has subsided ~0.65 km at the deepest point near the depocenter. The vertical relief of Red-1 due to faulting and folding across the NAF-N is also 0.65 km (Figure 2b). This implies a differential subsidence of ~6.0 mm/yr. Total subsidence could be greater if the onlap point for Red-1 in the south is subsiding. Green-6 horizon is currently below 5 km depth at its depocenter (Figures 3, 4, and S2). Assuming that it was deposited at 1000 m water depth (Text S2), subsidence rates would average 7.4 mm/yr since 540 ka. We assign an uncertainty of 50 ka for the age of Red-1, and 10% for the depth conversion below the precisely known seafloor. A Holocene subsidence rate of 7.7 ± 1.3 mm/yr at the Cinarcik depocenter was independently deduced from the scarp morphology and shallow subbottom deformation along the NAF-N [*Seeber et al.*, 2006]. *Armijo et al.* [2005] calculated latest Pleistocene-Holocene rates of vertical separation as high as 6 mm/yr across faults in Central basin.

[13] Many authors have recognized a series of short NNE-dipping and left-stepping normal-separation faults along the southern wall of Cinarcik Basin, subparallel in strike to the NAF-N on the opposite side of the basin (Figures 1 and 2b) [*Le Pichon et al.*, 2001; *Armijo et al.*, 2002]. From precise measurement of fault dips and dip-slip components, we estimate only 261 m of extension by these faults perpendicular to the local strike of the NAF-N since deposition of Red-1 horizon or 2.4 mm/yr given the 109 ka model age for Red-1. Uncertainty for extension measures for each fault is ~2 m, with ~5 m for the two southern faults in Figure 2b. This contribution is much smaller than the 8–10 mm/yr extension predicted from the geometry and kinematics of the NAF-N [*Le Pichon et al.*, 2001, 2003], leaving 5.6 to 7.6 mm/yr of extension not accounted for. If the NAF-N is nonvertical, the demonstrated 7.4 mm/yr of subsidence requires extension across it, with the magnitude of this extension dependent on fault dip. For a subsidence of 7 mm/yr, this cross-fault extension would be 2.5, 4.0, and 7.0 mm/yr for a fault dipping, respectively, 70°, 60°, or 45°. Thus, a NAF-N that is an oblique right-normal fault in the releasing segment between the Tuzla and Istanbul bends can account for all the observations.

4. Summary and Conclusions

[14] Seismic stratigraphic analysis in the Cinarcik Basin documents a time-transgressive depocenter that migrated smoothly westward by 8 km during the last 487 ka. This observation supports the model of basin formation at releasing transform bends proposed by *Seeber et al*. [2010]. In that context, our results indicate steady state dextral slip on the NAF-N over the last 0.5 Myr (Figure 4). This rate is consistent with a steady rate of vertical motion for the same time interval across the NAF-N in Kumburgaz Basin to the west [*Sorlien et al*., 2012]. It is not consistent with a proposed new NAF-N cutting through and deactivating pull-apart basins at about 200 ka, and accumulating only about 4 km of slip [*Le Pichon et al*., 2003].

[15] Assuming steady plate motion at the current GPS rates of 23–24 mm/yr, the preferred 18.5 mm/yr right displacement on the Cinarcik segment of the NAF-N implies that the combined displacement on other NAF branches to the south has been about 4.5–5.5 mm/yr, within the uncertainties of this study. This is important to earthquake hazard evaluations for cities and towns near the onshore parts of these other fault branches.

[16] At the Tuzla extensional bend, the NAF dips to the south below the basin and accommodates extension as well as subsidence by oblique slip. In combination with the 2.4 mm/yr of extension, we measured across the southern extensional field, 8–10 mm/yr total extension expected at the extensional bend [*Le Pichon et al*., 2003] can be accommodated by the NAF-N if its dip is 45° and vertical motion is 7 mm/yr. A steeper fault dip would mean some extension is accommodated by layer-parallel stretching or some unidentified process. The large vertical component of slip we have documented suggests a high potential for tsunami from ruptures of the 30 km long Tuzla-Istanbul releasing segment of the NAF-N. Indeed, historical tsunamis have caused damage to Marmara Sea coasts and populations [*Altınok and Ersoy*, 2000].

[17] Lastly, the oldest interpreted depocenter derived from subsidence at the Tuzla bend is now near the Istanbul bend, ~30 km from where it originated [*Carton et al*., 2007] (Figure 1). Extrapolating backward in time our preferred 18.5 mm/yr rate, this displacement implies a minimum 1.6 Ma age for the Cinarcik Basin.

[18] **Acknowledgments.** Funding for this work was provided by Post Doctorate Research Fellowship Program of the Scientific and Technological Research Council of Turkey (TUBITAK), Research Abroad Fellowship of Istanbul Technical University and National Science Foundation (grants OCE-03-28118, OCE 03–28119, OCE-03-27273, OCE 09–28447, and OCE-09-29063). We would like to thank captains and crews, and scientific parties of SeisMarmara and TAMAM 2010 PirMarmara leg a4. We thank Hydroscience Technologies, Inc. for their valuable support for the seismic systems of Piri Reis and Promax (Halliburton) and Focus (Paradigm Geophysical) software programs for data processing. SPW from Parallel Geoscience was used for additional data processing. IHS donated "the Kingdom Suite" software to all five involved universities, which we used extensively for interpretation and graphics. Lamont-Doherty Earth Observatory publication 7720.

[19] The Editor thanks Mustapha Meghraoui for his assistance in evaluating this paper.

References

Altınok, Y., and S. Ersoy (2000), Tsunamis observed on and near Turkish coast, *Nat. Hazards*, *21*(2–3), 185–205.

Ambraseys, N., and C. Finkel (1995), *The Seismicity of Turkey and Adjacent Areas, A Historical Review, 1500–1800*, 240 pp., EREN, Istanbul, Turkey.

Ambraseys, N. N., and J. A. Jackson (2000), Seismicity of the Sea of Marmara (Turkey) since 1500, *Geophys. J. Int*, *141*, F1–F6.

Armijo, R., B. Meyer, S. Navarro, G. King, and A. Barka (2002), Asymmetric slip partitioning in the Sea of Marmara pull-apart: A clue to propagation processes of the North Anatolian Fault?, *Terra Nova*, *14*, 80–86.

Armijo, R., et al. (2005), Submarine fault scarps in the Sea of Marmara pull-apart (North Anatolian Fault): Implications for seismic hazard in Istanbul, *Geochem. Geophys. Geosyst.*, *6*, Q06009, doi:10.1029/2004GC000896.

Barka, A., and K. Kadinsky-Cade (1988), Strike-slip fault geometry in Turkey and its influence on earthquake activity, *Tectonics*, *7*, 663–684.

Brocher, T. M. (2005), Empirical relations between elastic wavespeeds and density in the Earth's crust, *Bull. Seismol. Soc. Am.*, *95*, 2081–2092.

Carton, H., et al. (2007), Seismic imaging of the three-dimensional architecture of the Cinarcik Basin along the North Anatolian Fault, *J. Geophys. Res.*, *112*, B06101, doi:10.1029/2006JB004548.

Cormier, M.-H., et al. (2006), North Anatolian Fault in the Gulf of Izmit (Turkey): Rapid vertical motion in response to minor bends of a nonvertical continental transform, *J. Geophys. Res.*, *111*, B04102, doi:10.1029/2005JB003633.

Crowell, J. C. (Ed.) (2003), *Evolution of Ridge Basin, Southern California: An Interplay of Sedimentation and Tectonics*, vol *367*, 247 pp., Special Publication Geological Society of America.

Dessa, J., H. Carton, and S. C. Singh (2007), Structural insight of the Eastern Marmara Sea by combined multichannel seismic and refraction tomography, *Eos Trans. AGU*, *88*(52), T31C–0595.

Dolan, J. F., D. D. Bowman, and C. G. Sammis (2007), Long-range and long-term fault interactions in southern California, *Geology*, *35*(9), 855–858.

Emre, O., T. Y. Duman, S. Ozalp, H. Elmaci, S. Olgun, and F. Saroğlu (2012), Active fault map of Turkey with an exploratory text, in *Mineral Research and Exploration (MTA),* General Directorate of MTA Special Publication Series, Ankara, Turkey.

Frankel, K. L., J. F. Dolan, L. A. Owen, P. Ganev, and R. C. Finkel (2011), Spatial and temporal constancy of seismic strain release along an evolving segment of the Pacific-North American plate boundary, *Earth Planet. Sci. Lett.*, *304*, 565–576.

Gasperini, L., A. Polonia, N. Cagatay, G. Bortoluzzi, and V. Ferrante (2011), Geological slip rates along the North Anatolian Fault in the Marmara region, *Tectonics*, *30*, TC1010, doi:10.1029/2011TC002906.

Kozaci, O., F. J. Dolan, and R. C. Finkel (2009), A late Holocene slip rate for the central North Anatolian fault, at Tahtaköprü, Turkey, from cosmogenic 10Be geochronology: Implications for fault loading and strain release rates, *J. Geophys. Res.*, *114*, B01405, doi:10.1029/2008JB005760.

Kurt, H., and E. Yucesoy (2009), Submarine structures in the Gulf of İzmit, based on multichannel seismic reflection and multibeam bathymetry, *Mar. Geophys. Res.*, *30*, 73–84.

Le Pichon, X., et al. (2001), The active main Marmara fault, *Earth Planet. Sci. Lett.*, *192*, 595–616.

Le Pichon, X., N. Chamot-Rooke, and C. Rangin (2003), The North Anatolian fault in the Sea of Marmara, *J. Geophys. Res.*, *108*(B4), 2179, doi:10.1029/2002JB001862.

Meghraoui, M., M. E. Aksoy, H. S. Akyuz, M. Ferry, A. Dikbas, and E. Altunel (2012), Paleoseismology of the North Anatolian Fault at Güzelköy (Ganos segment, Turkey): Size and recurrence time of earthquake ruptures west of the Sea of Marmara, *Geochem. Geophys. Geosyst.*, *13*, Q04005, doi:10.1029/2011GC003960.

Okay, A. I., A. Kaslilar-Ozcan, C. Imren, A. Boztepe-Guney, E. Demirbag, and I. Kuscu (2000), Active faults and evolving strike-slip basins in the Marmara Sea, Northwest Turkey: A multichannel seismic reflection study, *Tectonophysics*, *321*, 189–218.

Polonia, A., et al. (2004), Holocene slip rate of the North Anatolian Fault beneath the Sea of Marmara, *Earth Planet. Sci. Lett.*, *227*, 411–426.

Rangin, C., E. Demirbag, C. Imren, A. Crusson, A. Normand, E. Le Drezen, and A. Le Bot (2001), *Marine Atlas of the Sea of Marmara (Turkey)*, Ifremer, Plouzané, France.

Rangin, C., X. Le Pichon, E. Demirbag, and C. Imren (2004), Strain localization in the Sea of Marmara: Propagation of the North Anatolian Fault in a now inactive pull-apart, *Tectonics*, *23*, TC2014, doi:10.1029/2002TC001437.

Reilinger, R., and S. McClusky (2011), Nubia–Arabia–Eurasia plate motions and the dynamics of Mediterranean and Middle East tectonics, *Geophys. J. Int.*, *186*(3), 971–979.

Seeber, L., O. Emre, M.-H. Cormier, C. C. Sorlien, C. M. G. McHugh, A. Polonia, N. Ozer, and N. Cagatay (2004), Uplift and subsidence from oblique slip: The Ganos-Marmara bend and the North Anatolian Transform, western Turkey, *Tectonophysics*, *391*, 239–258.

Seeber, L., M.-H. Cormier, C. McHugh, O. Emre, A. Polonia, and C. C. Sorlien (2006), Rapid subsidence and sedimentation from oblique slip near a bend on the North Anatolian transform fault in the Marmara Sea, Turkey, *Geology*, *34*, 933–936.

Seeber, L., C. C. Sorlien, M. S. Steckler, and M.-H. Cormier (2010), Continental transform basins: Why are they asymmetric?, *Eos Trans. AGU*, *91*, 29–30.

Shillington, D. J., et al. (2012), Evidence for widespread creep on the flanks of the Sea of Marmara transform basin from marine geophysical data, *Geology*, *40*, 439–442.

Sorlien, C. C., et al. (2012), Uniform basin growth over the last 500 ka, North Anatolian Fault, Marmara Sea, Turkey, *Tectonophysics*, *518–521*, 1–16.